# Robust and High-Performance Textile-based Triboelectric Nanogenerators Integrated with 2D Materials for Sustainable Self-Powered Wearable Electronics

*Iftikhar Ali, Nazmul Karim* and Shaila Afroj**

I. Ali, Prof. N. Karim, and Dr. S. Afroj
Centre for Print Research (CFPR), The University of the West of England, Bristol, BS16 1QY, UK. E-mail: shaila.afroj@uwe.ac.uk.

Prof. N. Karim
Nottingham Trent University, Shakespeare Street, Nottingham, NG1 4GG, UK.
Email: nazmul.karim@ntu.ac.uk

## Abstract

The human body continuously generates ambient mechanical energy through diverse movements, such as walking and cycling, which can be harvested *via* various renewable energy harvesting mechanisms. Triboelectric Nanogenerator (TENG) stands out as one of the most promising emerging renewable energy harvesting technologies for wearable applications due to its ability to harness various forms of mechanical energies, including vibrations, pressure, and rotations, and convert them into direct current (DC) electricity. However, their application is limited due to challenges in achieving performance, flexibility, low power consumption, and durability. Here, we present a robust and high-performance self-powered system integrated into cotton fabric by incorporating a textile-based triboelectric nanogenerator (T-TENG) based on 2D materials, addressing both energy harvesting and storage. The proposed system extracts significant ambient mechanical energy from human body movements and stores it in a textile supercapacitor (T-Supercap). The integration of 2D materials (graphene and $MoS_2$) in fabrication enhances the performance of T-TENG significantly, as demonstrated by a record-high open-circuit voltage of 1068V and a power density of 14.64 W/m$^2$ under a force of 22N. The developed T-TENG in this study effectively powers 200+ LEDs and a miniature watch while also charging the T-Supercap with 4-5N force for efficient miniature electronics operation. Integrated as a step counter within a sock, the T-TENG serves as a self-powered step counter sensor. This work establishes a promising platform for wearable electronic textiles, contributing significantly to the advancement of sustainable and autonomous self-powered wearable technologies.

## Introduction

Wearable electronic textiles (e-textiles) and the Internet of Things (IoT) have encouraged extraordinary developments, stimulating advances in biosensors, smart wearable systems, and cutting-edge solutions for healthcare and portable electronics.[1-3] The rise in the number of sensors in e-textile devices promptly correlates with an increase in power demand. However, existing power sources, such as rechargeable or electrochemical batteries, are not only rigid and bulky but also suffer from short lifespans, posing significant barriers to the scalability of wireless sensors and wearable devices.[4-6] There remains an urgent unmet need for a sustainable, flexible, wearable and durable power source for wearable e-textiles.[7, 8] Furthermore, the rapid trend towards miniaturisation, as well as the growing emphasis on wearability in portable electronics, needs a fundamental re-evaluation of both design principles and operational requirements.[9, 10]

Triboelectric Nanogenerator (TENG) stands out as one of the most promising emerging renewable energy harvesting technologies for wearable applications.[11] Such devices are capable of harnessing diverse forms of mechanical energy like vibrations, pressure, and rotations, and converting them into direct current (DC) electricity. Triboelectric charges build on the surfaces where two different materials with dissimilar electron affinities meet under mechanical stress or deformation, resulting in the generation of a potential difference between the two electrodes and can be utilized directly to power electronics like LEDs or mini watches.[12, 13] Additionally, the electricity generated can be stored in electrochemical batteries or supercapacitors, enabling the operation of various portable devices.[14] Textile-based TENGs have recently emerged as self-powered sources for e-textile applications, attracting considerable attention due to its lightweight, flexible and wearable nature.[15-17] However, their low power-generating capabilities indicate ample opportunity for further development in creating self-sufficient power sources for wearable e-textiles.[18]

Recently, there has been a significant focus on two-dimensional (2D) materials in the development of diverse energy harvesting devices.[3] The versatile role of these materials encompasses their utilization as electrodes, buffer layers, and performance enhancers, notably in terms of efficiency and durability.[19] Moreover, the application of 2D materials in the development of TENGs has attracted significant attention, with various 2D materials being employed to augment the performance of these devices.[20] Significant progress has been made in the development of wearable TENG devices based on 2D materials. However, notable challenges persist, particularly concerning the poor durability and stability of these devices.[21] Additionally, research on textile-based TENGs using 2D materials for self-power applications remains lacking, highlighting the critical need for focused studies aimed at enhancing both the lifespan and power generation capabilities of textile-based TENGs.

Here we report the development and utilization of a textile-based self-powered system, combining both T-TENG and T-Supercap. The primary objective revolves around enhancing the output efficiency of T-TENG through the integration of 2D materials, notably utilizing graphene as electrodes and introducing 2D $MoS_2$ to augment device performance. The pivotal use of triboelectrification insulator-coating materials (positive) in tandem with thin Kapton tape (negative) facilitates the crucial triboelectrification process. In the textile-based supercapacitor realm, graphene serves as the principal electrode, complemented by an ionic electrolyte. The resultant T-TENG device showcases a remarkable capability, generating an excess of 1068V in open circuit voltage ($V_{OC}$), illuminating more than 200 commercial LEDs interconnected in a series configuration. Furthermore, the T-TENG is capable of charging nine T-Supercaps in series to 10V in 250s employing a 7-10N force and a frequency of 4-6Hz. Notably resilient, the device sustains over 45% of its outputs even after a continuous operation span of 7 months. Moreover, when affixed to diverse body parts, it exhibits a potential to

generate over 482V $V_{OC}$ during walking, demonstrating its viability for practical integration within wearable technologies.

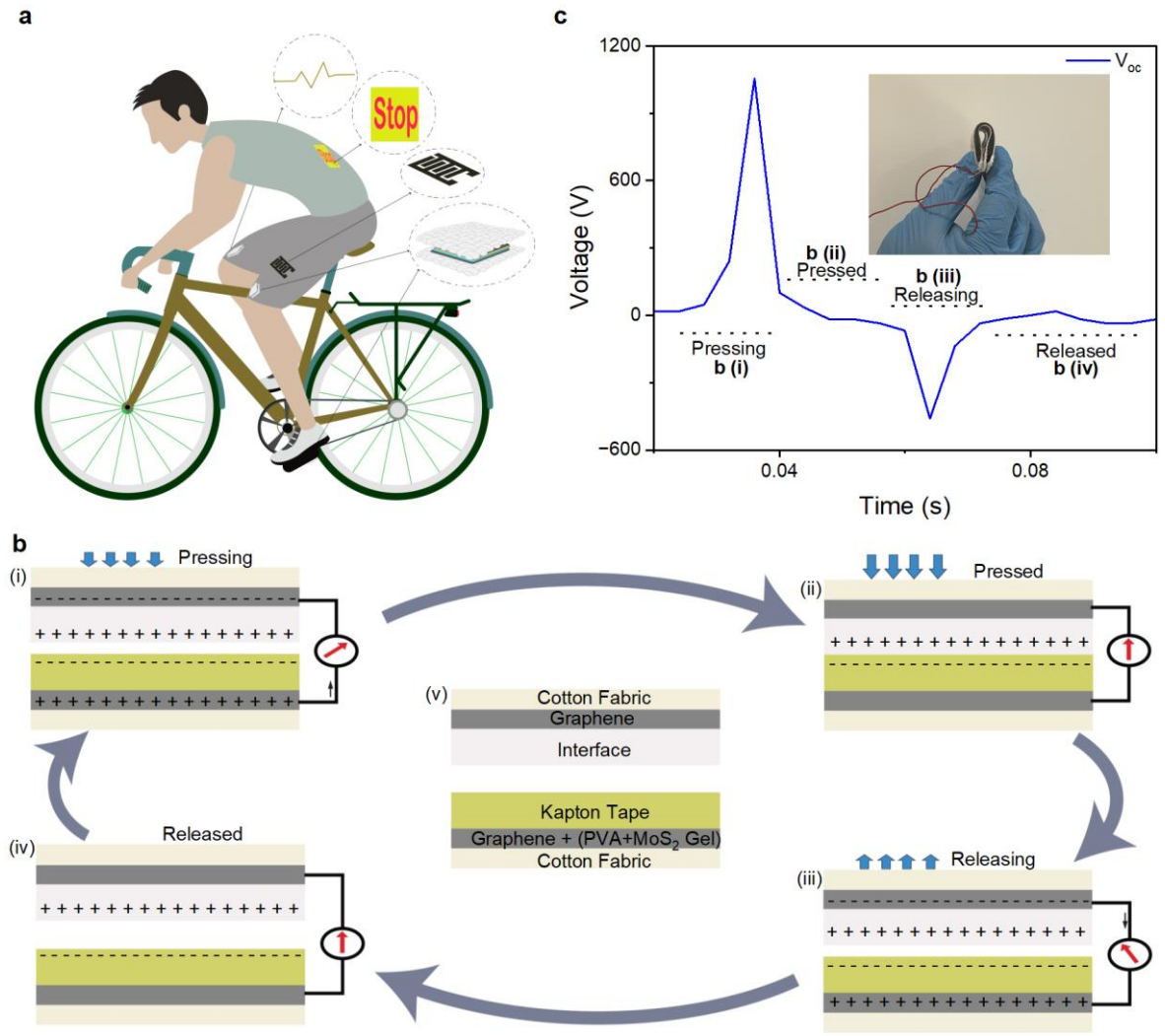


**Figure 1:System overview and working mechanism of T-TENG;** (a) Schematic illustration of integrated self-powered system, where a cyclist wearing a dress having energy harvesting (T-TENG), storage (T-Supercap) and real-time applications (Powering LEDs and counting steps). (b) Configuration of the developed T-TENG (middle), working mechanism: (i) pressing, (ii) pressed, (iii) releasing, (iv) released state and (v) the configuration of T-TENG. (c) the corresponding output curve in response to each step in (b).

## Results and Discussion

### System Overview and Working Mechanism of T-TENG

In this tech-driven era, imagine harvesting ambient energy from human motion to power wearable devices like a cyclist's shirt with built-in energy harvesting and storage system **(Figure 1a)**. This approach eliminates complex circuits, promising cost-effective maintenance and paving the way for a more sustainable energy solution for wearable sensors and portable electronics. A comprehensive overview of the T-TENG configurations used in this study and their working mechanisms is presented in **Figure 1b**. The proposed T-TENGs operate on contact separation mode based on the triboelectric effect, where two dissimilar materials with different electron affinities generate opposite charges when they come into contact. These charges are then collected through electrodes and recombined after passing through a load. Similarly, when force is applied to the T-TENG device, where during a pressing mode, a high peak is generated. Each step in **Figure 1b** corresponds to an illustrated output in **Figure 1c**. This peak returns to 0 as long as the T-TENG tribo-layers remain pressed and in contact due to the lack of separation of charges. Upon release, a negative voltage peak occurs due to the built-in electric field among the layers. This process, demonstrated through **Figures 1b and 1c**, allows for the cyclic generation of electricity by pressing and releasing the T-TENG device.

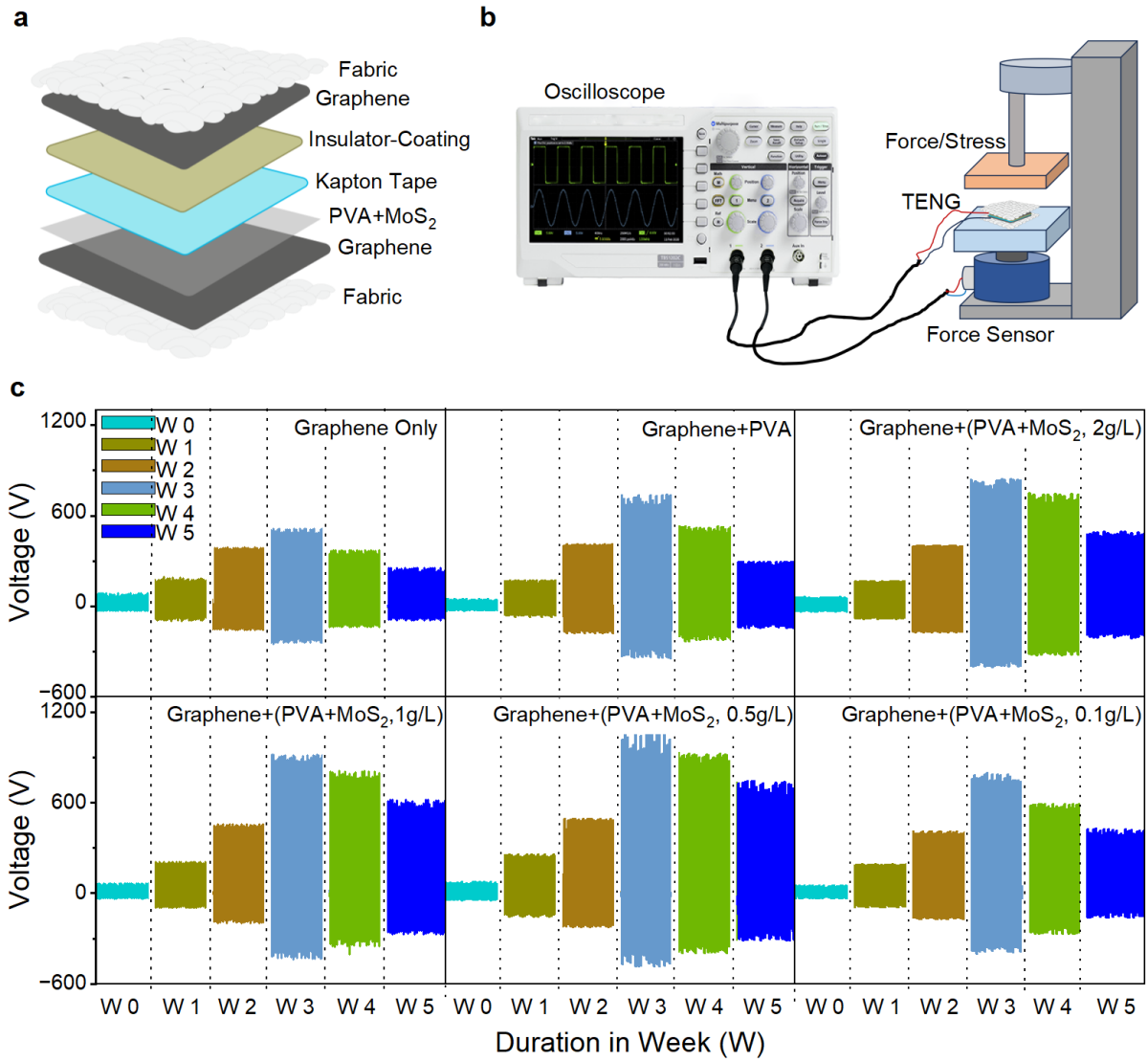


**Figure 2: Output Performance;** (a) the schematic of the developed T-TENG, highlighting its diverse layers. (b) The accompanying measurement setup comprise of an oscilloscope and a force machine equipped with force measurement capabilities. (c) the output response of the developed T-TENGs subjected to a 22N force at a frequency of 5-7 Hz, tracked from day 1st to the end of week 5. These devices exhibit variations in $MoS_2$ ratios while maintaining a consistent overall configuration.

### 1.1.Influencing Factors on Output Performance

The structural parameters of the T-TENG can be fine-tuned based on specific requirements, including materials, gap dimensions, layer thickness, and more. This section will first showcase how the incorporation of the 2D material ($MoS_2$) positively impacts performance and subsequently investigate other influential factors affecting the performance of T-TENG.[20] Six devices are developed with the following configuration: Fabric/Graphene/Insulator-coating (Tribo-material 1)/Spacer (sponge)/ Fabric/Graphene/PVA-$MoS_2$ composite gel/ Kapton tape (Tribo-material 2) **(Figure 2a)**. These devices are designed to investigate the impact of polyvinyl alcohol-$MoS_2$ (PVA+$MoS_2$) gel with varying concentrations of $MoS_2$ (2g/L, 1g/L, 0.5g/L and 0.1g/L in water), as well as one device with only PVA gel and one without any gel. In the upper section of the T-TENG, graphene serves as the electrode on a cotton fabric substrate, while an insulator paste material is utilised as the positive tribo-layer. Proceeding to the bottom section of the T-TENG, a graphene electrode layer fabricated on a cotton fabric, forming a combination with a PVA+$MoS_2$ gel layer. This gel layer incorporates varying concentrations of $MoS_2$, strategically designed to augment the capacity and long-term cycling performance of the graphene electrode.[22] Kapton tape functions both as the negative tribo-layer and an encapsulating layer. The integration of the upper and lower sections of the T-TENG is facilitated by employing a sponge as a spacer, enhancing the triboelectric effect in contact separation mode. The open-circuit voltage ($V_{oc}$) of these devices was characterized using a specialized stress machine assembled in the lab, equipped with various force-exerting, and measuring capabilities, along with a digital oscilloscope **(Figure 2b)**. The output results ($V_{oc}$) of these T-TENGs were obtained at weekly intervals (W), starting from the first day of fabrication and continuing until the fifth week **(Figure 2c)**. The measurements were conducted with a frequency of 6–8 Hz and a force of 20–22 N. The results consistently showed improvement until week 3 (W3) due to several factors. The repeated application of force

resulted in a tighter contact between the tribo-layer and the conductive electrode (graphene), promoting stronger bonding and higher charge accumulation. As time passed, the drying of the layers reduced internal charge recombination, positively influencing the output results. However, a decline in performance was noted after week 4 (W4). This decrease was attributed to issues such as the residual adhesiveness of Kapton tape leaving contamination on the graphene layer, leading to reduced adhering and reduced charge accumulation.[23] Additionally, continuous bending and stress caused surface cracks that confirm from scanning electron microscopy (SEM) images, elevating sheet resistance and parasitic capacitance and further decreasing the output results **(Figure S1-2, supporting information).** Additionally, the environmental humidity also impacts the device's performance by facilitating the adherence of water molecules to the triboelectric surface. This adherence leads to the dissipation of charge, thereby reducing the charge density on the material surface and consequently compromising the device's output performance.[24] However, Despite these challenges, the decreasing ratio with time is observed smaller after W5, and even after seven months, these devices still retain the ability to generate around 45% of the peak results achieved after W3 **(Figure S3, supporting information)**, demonstrating the high durability of the fabricated T-TENG.

As illustrated in **Figure 2c**, the incorporation of $MoS_2$ significantly improved the output performance of the T-TENG device. A comparison of the inclusion of PVA gel to that of only graphene electrode are studied and observed an elevation of 17.67% increase in the output results comparing to that of graphene only. The boosted results can be due to PVA's strong dielectric characteristics, which successfully increased the surface's tribo-positive polarity.[25] Similarly, the addition of $MoS_2$ at a concentration of 0.1g/L in composition with PVA in a ratio of 1:1 (PVA+$MoS_2$, 0.1g/L) resulted in 21.31% improvement in output performance compared to the T-TENG with only graphene. Moreover, elevating the concentration of $MoS_2$, particularly at 0.5g/L in the composite (PVA+$MoS_2$, 0.5g/L), enhanced the device performance

significantly, demonstrating an improvement of approximately 34.94% compared to T-TENG solely incorporating graphene, and 18.40% increase compared to that T-TENG based on only the PVA layer on the graphene electrode. T-TENGs with further higher concentrations of $MoS_2$ such as 1g/L and 2g/L, generated high voltages compare to those without $MoS_2$. However, their output voltages remained below that of T-TENG containing a 0.5g/L $MoS_2$ concentration. This observation is likely linked to the inherent characteristics of the 2D material $MoS_2$.[26] Initially, the quantity of $MoS_2$ impacts the electrochemical properties of the graphene-$MoS_2$ composite electrode. While a high $MoS_2$ concentration decreases electrical conductivity, it also leads to the aggregation of $MoS_2$ on the graphene layer. Conversely, a low $MoS_2$ concentration contributes less to the overall capacity and graphene accumulation, thereby affecting the output results.[26] Consequently, achieving a balance in concentration emerged as a crucial factor in our study, ultimately yielding an optimized voltage of approximately 1068V with a 0.5g/L $MoS_2$ concentration.

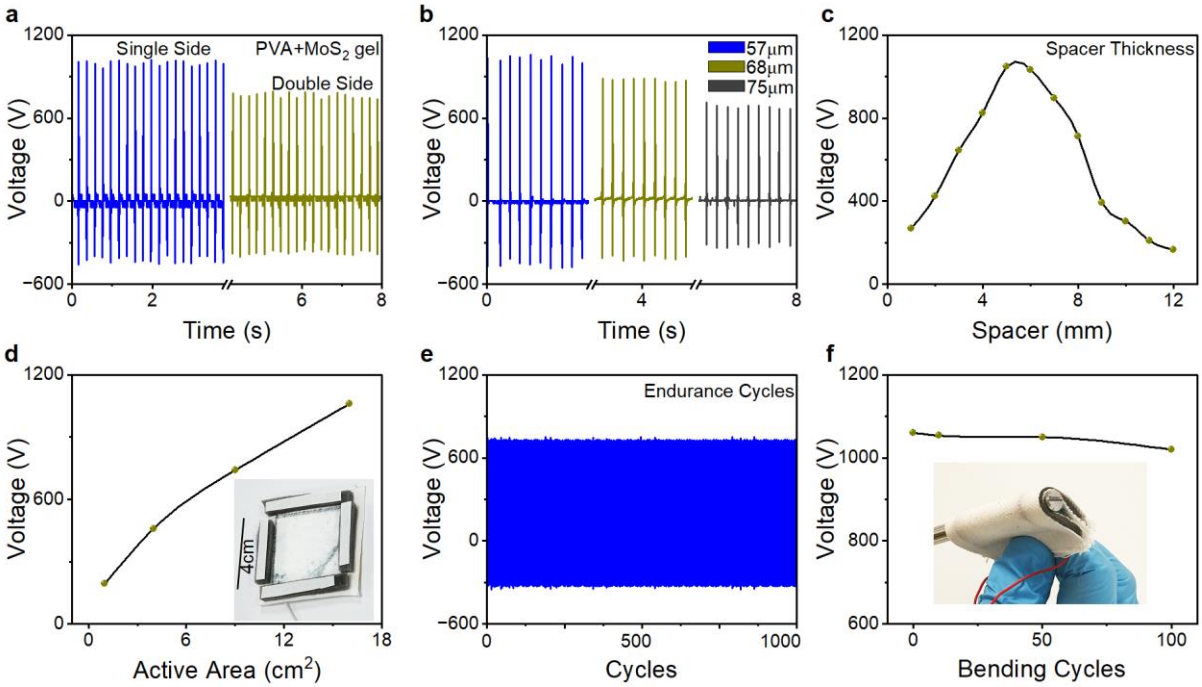


**Figure 3: The further optimization of the T-TENG involved various aspects:** (a) exploration of single-sided and double-sided PVA+MoS2 (0.5% wt.), (b) variation in the

thickness of the insulator-coating layer (tribo-layer), (c) examination of the effect of spacer size on output, (d) investigation of the response of output with increasing T-TENG activation, with the inset displaying the active area of the T-TENG top section, (e) endurance testing of the T-TENG device through approximately 1000 cycles under a 14N force with a frequency of 5-7 Hz, and (f) a demonstration of flexibility through 100 bending cycles with an 8mm radius of curvature, as illustrated in the inset photo of the T-TENG bending around an 8mm diameter rod.

Following material optimisation, structural optimisation was undertaken to augment the T-TENG output response. A T-TENG device was constructed with PVA+$MoS_2$ (0.5 g/L) on both sides. The T-TENG device with one side PVA+$MoS_2$ (0.5g/L) performed better than the T-TENG with two sides PVA+$MoS_2$ (0.5g/L) by about 8.87% **(Figure 3a)**. This difference might explain the similarities in the composition of both electrodes since the major goal of the composite PVA+$MoS_2$ gel was to improve the triboelectric effect and aid in charge separation. With comparable compositions on both sides, comparatively weak electric field is established within T-TENG and leading in reduced overall output performance.[27] The investigation further explored optimising the performance of T-TENG by exploring the potential impact of tribo-layer thickness. Varied thicknesses of insulator-coating materials (tribo-layer) were examined, revealing an optimal thickness of approximately 57µm. Intriguingly, further increases in thickness led to a decline in T-TENG performance **(Figure 3b)**. This phenomenon is attributed to surpassing an optimum thickness, resulting in a reduction in charge density.[28] The performance of TENGs relies significantly on the distance or space between tribo-layers. To determine the optimal spacer thickness for our T-TENG, we varied the thickness from 1 mm to 12 mm. The observations revealed a notable enhancement in output voltage with increasing spacer (sponge) thickness, reaching a peak at 5.5 mm. However, a further increase in spacer thickness resulted in a decline of output voltage. Thus, the findings depicted in **Figure**

**3c** demonstrate the critical importance of selecting an optimum spacer thickness, a notion supported by various studies.[4] To determine the influence of active area on the performance of the device, T-TENGs were constructed with four different active areas and subjected to a 22N force. A linear increasing trend in the output was observed, as the active areas were progressively enlarged **(Figure 3d)**. The developed T-TENGs demonstrated exceptional endurance, withstanding characterization under a 14N strain for more than 1000 cycles. Throughout testing, the output displayed steady performance with barely any decline **(Figure 3e)**. To test wearability and flexibility, the devices were bent with an 8-mm radius of curvature, and the devices retained an amazing 96% of their output even after 100 bending cycles **(Figure 3f)**. These findings highlight the T-TENG device's potential for usage in a variety of long-term applications, notably in wearable technologies.

**Electrical Performance of the Optimized T-TENG**

The optimisation of the T-TENG results in a final design that includes $MoS_2$ on one side and a 5.5 mm thick spacer. The tribo-layer, composed of an insulator-coating material, is kept at an optimal thickness of 57μm. The $V_{oc}$ of the optimised T-TENG was explored in relation to different forces to assess its potential for integration into diverse wearable positions like elbow joints and shoes or socks. Increasing the force on the T-TENG led to a significant rise in output voltage, with the device achieving an output voltage exceeding 1070V at a force of 22N **(Figure 4a)**. Additionally, the response of the T-TENG to various frequencies was investigated using a 10N force, revealing a slight increase in output voltage with frequency. An increase of 1.2 times was observed up to 8Hz compared to 1Hz, but there was very minor increase above 9 Hz **(Figure 4b)**. These results emphasise the T-TENG's potential for implementation in

various wearable applications, offering the ability to harvest energy during activities such as walking, running, cycling, and more.

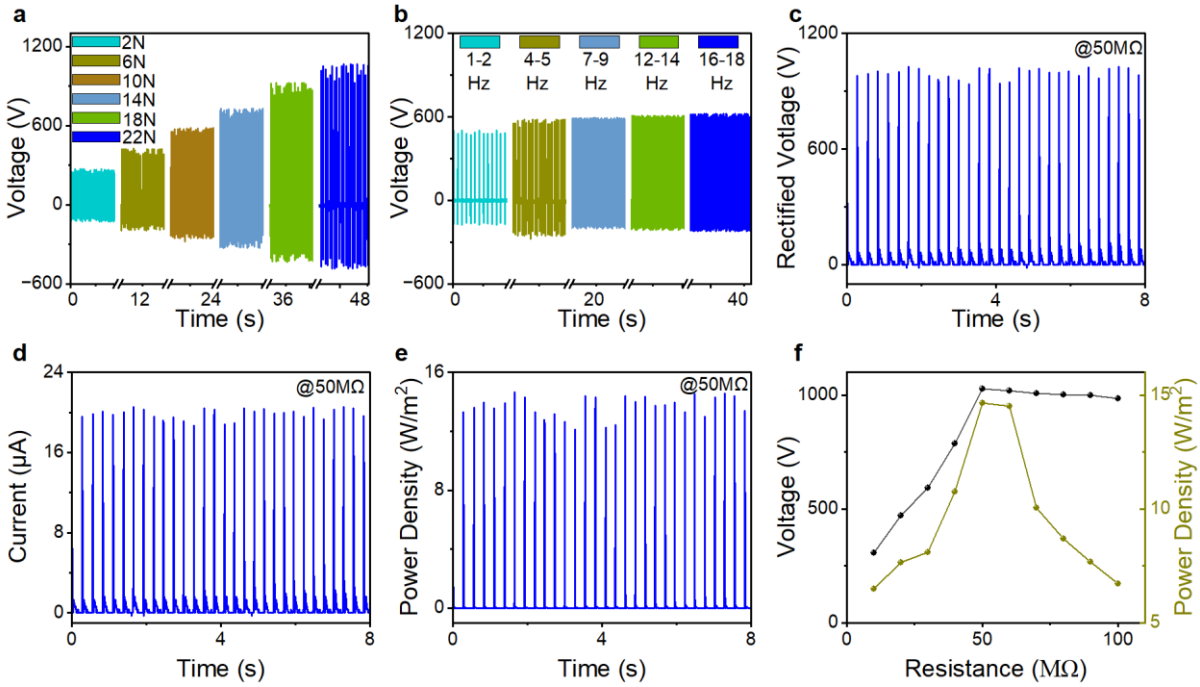


**Figure 4: Output performance of optimized T-TENG;** (a) Open circuit voltage in response to varying force, and (b) with varying frequency under 14N force. Rectified outputs at 50MΩ resistive load (c) Voltage, (d) Current, and (e) power density. (f) the output voltages and power densities response to various resistive load from low to high.

The optimised T-TENG was subjected to further characterization under various resistive loads, revealing a rectified output voltage of approximately 1028 under a 22N force across a 50MΩ load with a calculated current of approximately 20.2 μA **(Figures 4c and 4d)**. The power density was computed and found around 14.64 W/m$^2$ **(Figure 4e)**. Numerous studies have found encouraging findings for textile-based triboelectric nanogenerators (TENGs). Notably, the findings of this study stand out as having the highest reported values among cotton fabric based TENGs. To support these findings, a comparison table **(Table 1)** is presented, which includes results from previously published publications on T-TENGs. Investigating the T-TENG's response to different resistive loads, measurements of rectified voltage and power

densities were conducted across a range from 1MΩ to 100MΩ. A linear increase in both power densities and voltage was observed up to 50 MΩ; however, a further increase in the load led to reduction in power densities **(Figure 4f)**. These characterizations demonstrate the potential of T-TENGs for applications requiring high loads.

**Table 1:** Performance comparison with recently published textile based TENGs.

| Materials/Substrates | $V_{OC}$ (V) | Power Density ($W/m^2$) | Year/Ref |
|---|---|---|---|
| Woven conductive textile, Si-rubber, Silk, knitted conductive textile | 28.13 | 0.166 | 2017, [29] |
| Black phosphorus, cellulose-derived hydrophobic nanoparticles, PET Fabric | 880 | 5.2 | 2018, [30] |
| Nylon fabric, Ag electrodes, fabric, Acrylic, polyvinyl chloride | 136 | 0.0388 | 2019, [31] |
| Fluorinated ethylene propylene, Nylon, Ag, tape | 120 | 0.0465 | 2019, [32] |
| Cyanoalkyl silane, fluoroalkyl silane, silver, Cotton, Silk | 216.8 | 3.45 | 2021, [33] |
| Wrap Ag electrode, polytetrafluoroethylene vinyl fabric, nylon fabric | 62.9 | 0.0053 | 2022, [34] |
| Graphene, Polydimethylsiloxanes, Polyamide textile, PET substrate | 71 | 0.0308 | 2023, [35] |
| Coper wires, Acetate cloth, Yarn, Ecoflex | 361.4 | 0.792 | 2023, [36] |
| Ag-absorbed cotton, Cu-plated cotton, Pristine Cotton, Plant fibre | 25 | 0.7225 | 2023, [37] |
| Graphene, $MoS_2$, Insulator-coating, Kapton tape, Cotton fabric | 1068 | 14.64 | **This Work** |

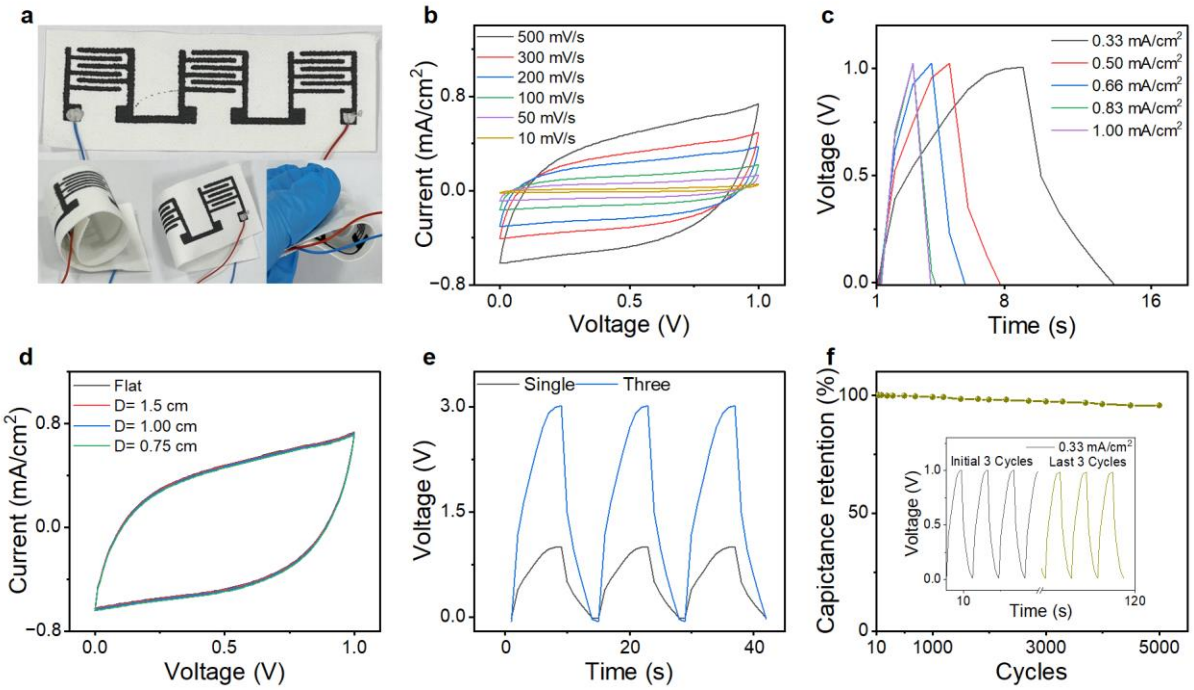


**Figure 5: Energy storage unit;** (a) photographs of textile-based supercapacitors, where three symmetric supercapacitors in series in flat and various bending shapes. (b) CV curves for various scan rate and (c) GCD curves with various current densities. (d) CV curves recorded with scan rate of 500 mV/cm$^2$ under flat and three different bending radii. (e) GCD curves of single and three supercapacitors connected in series, and (f) the capacitance retentions after various cycles, while inset showing the initial and final three GCD cycles.

**Energy Storage Unit: Textile supercapacitors**

As part of making a fully self-powered energy system, an energy storage unit was achieved through the development of in-plane symmetrical textile-based supercapacitors (three in series), utilising graphene as the electrode material and PVA gel as the electrolyte. Each individual supercapacitor comprises three branches, each having a length of 22.6mm and a width of 1mm on both the anode and cathode, separated by a 1mm gap from neighbouring electrodes. A photograph of the fabricated device highlights three textile-based symmetric-type supercapacitors arranged in series with differing bending shapes that showcase the flexibility

of the devices, as illustrated in **Figure 5a**. The electrochemical performance of the fabricated T-Supercaps was assessed through cyclic voltammetry (CV) and galvanometric charge-discharge (GCD) analyses. CV curves, obtained at various scan rates (500 to 10 mV/s) for a single supercapacitor, consistently exhibited rectangular shapes, indicating the T-Supercap's quality resembled that of an ideal double-layer supercapacitor **(Figure 5b)**. In accordance with CV results, GCD for the developed T-Supercap was measured across current densities from 0.33 $mA/cm^2$ to 1.0 $mA/cm^2$, revealed triangular-shaped curves with nearly identical charge and discharge times, akin to an ideal double-layer supercapacitor **(Figure 5c)**. The calculated areal capacitance for a scan rate of 10 mV/s was found to be 4.9 $mF/cm^2$, which is more than the recently published results in ref [38]. To showcase the flexibility and stability of the device, the CV curves of the supercapacitor were measured while bending at various radius of curvature. Negligible effects were observed compared to the flat mode, indicating that the developed textile supercapacitor can be effectively employed for wearable applications in various positions on clothing **(Figure 5d)**. To assess the electrical combination response of the developed T-Supercaps, GCD curves were recorded for both a single supercapacitor and three supercapacitors in series. It was observed that for an equivalent charging time, the three supercapacitors in series reached 1V, while a single T-Supercap charged up to 3V. This confirms the linear and consistent behaviour in the fabricated supercapacitors, as illustrated in Figure 5e. The durability of the developed T-Supercap was validated by a cyclic run of GCD with a current density of 0.33 $mA/cm^2$ for over 1000 cycles. A minor reduction was observed, maintaining more than 96% capacitance retention **(Figure 6f).** These results highlight the potential of the developed T-Supercap for efficient energy storage applications.

**Integrated Self-powered system: Applications.**

Finally, the practical applications of T-TENG and textile supercapacitors were explored. **Figure 6a** illustrates a schematic for charging the developed textile supercapacitors via T-TENGs. The T-TENG output is rectified through rectifier circuits and then supplied to T-Supercaps. The system, as captured in the photograph **(Figure 6b)**, features nine T-Supercaps connected in series and being charged with a T-TENG through hand tapping. **Figure 6c** displays the charging curve of the series-connected textile supercapacitors, while a corresponding video clip, **(Clip1, supporting information)**, is included in the supporting information. The charging process to reach 10 volts took approximately 250 seconds, utilising a force of 7–10 N and a frequency of 4-6 Hz. Additionally, T-TENGs were utilised to charge commercial DC capacitors with values ranging from 1μF to 470μF, applying forces and frequencies of 8-10 N and 5-7 Hz, respectively. The T-TENG demonstrated a rapid charging capability, taking about 6 seconds to charge a 1μF capacitor up to 10V and approximately 60 seconds for a 470μF capacitor **(Figure 6d)**. Furthermore, T-TENGs were effectively employed with hand tapping to charge a 4.7μF capacitor, showcasing their potential for charging small portable electronics **(Clip2, supporting information)**. In addition to its energy storage applications, the T-TENG was harnessed for real-time step counting while walking or running, as seen in **Figure 6e (Clip 3, supporting information).** Its versatility was further demonstrated by illuminating indicators while cycling or walking, successfully lighting up over 160 commercial LEDs with just hand tapping, as showcased in **Figure 6f (Clip4, supporting information)**. Moreover, when placed and fixed in socks, the T-TENG generated an open-circuit voltage of approximately 480V during walking **(Figures 6g and 6h)**. This voltage output proved sufficient to power indicators with more than 120 LEDs while walking **(Clip 5, supporting information)**.

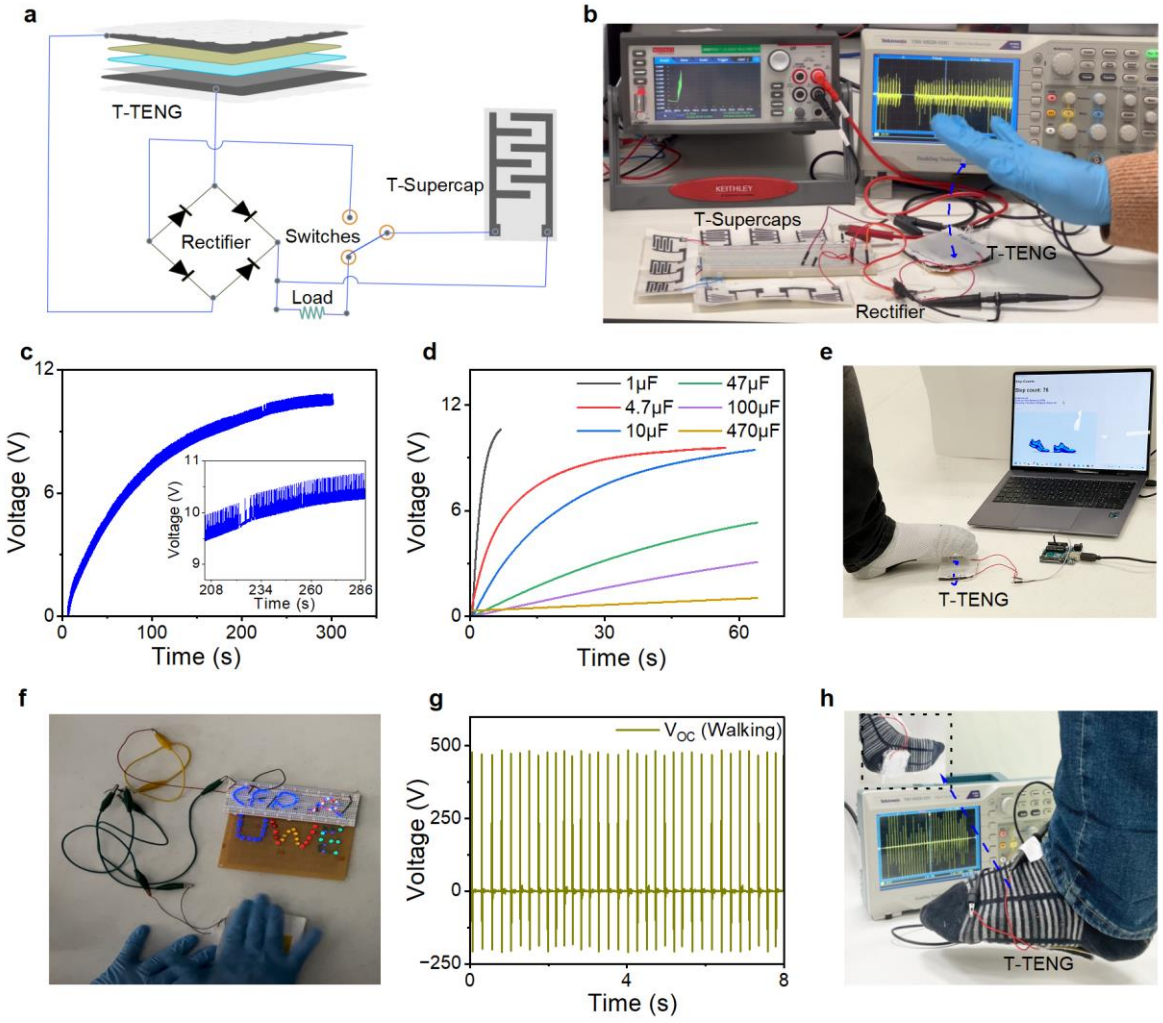


**Figure 6: Integrated self-powered system and real time applications; (**a) Schematic of charging setup for textile supercapacitor via T-TENG and (b) photograph of textile supercapacitors connected in series while charging with T-TENG. (c) The charging curve of the Textile supercapacitors connected in series with T-TENG. (d) The charging curves of commercial supercapacitors via T-TENG. (e) A photograph of step counting setup and (f) photograph of LEDs glowing while hand tapping T-TENG. (g) Output voltages during fixing while fixing T-TENG on socks and (h) photograph of the T-TENG fixed on socks.

## Conclusion

This systematic exploration into the application of 2D materials in textile-based energy harvesting and storage devices has resulted in the development of a highly efficient textile-based triboelectric nanogenerator (T-TENG). Leveraging 2D materials like graphene for electrodes and $MoS_2$ to enhance triboelectric performance, the optimised concentration of 0.5g/L in water demonstrated a substantial 2.5-fold improvement in output compared to T-TENG without MoS2. The device showcased exceptional flexibility and durability, sustaining 45% of its original performance even after six months. Complementing this, a textile-based supercapacitor for charge storage was created, effectively powering mini-electronics. The T-TENG also served as a step counter sensor and a reliable power source for LEDs, enabling real-time indications while walking or cycling. This self-powered system, developed on bare cotton textiles, opens avenues for the exploration of wearable e-textile applications, and marking a significant attention to further explore as sustainable energy solutions.

## Experimental Section

### Materials

Graphene (screen-printable ink) and $MoS_2$ dispersion in water, both with a concentration of 100 g/L, were purchased from Versarien$^{TM}$ plc, UK. sulfuric acid ($H_2SO_4$) (puriss, 95-97%) and PVA (molecular weight: 31 000-50 000, 98-99% hydrolysed) were purchased from Merck, UK. The cotton fabric, featuring a construction of (66×44/70×10) ×340, was kindly donated by Square Apparels Limited, Bangladesh. The screen-printable insulator-coating materials were acquired from Dycotec Materials Ltd (UK), while Kapton tape (25.4µm thick) was obtained from DigiKey UK.

## T-TENG Fabrication

Graphene was printed on cotton fabric as electrodes in a 4 cm by 4 cm pattern using a manual screen printer with a 63T mesh. After printing, it was dried in an 80 °C in a furnace for 10 minutes. Copper wires were then attached to the electrodes using silver paste. To make different concentrations of 2 g/L, 1 g/L, 0.5 g/L, and 0.1 g/L, the $MoS_2$ mixture was mixed with deionized water and stirred for two hours under ambient conditions. A PVA gel was prepared by dissolving in DI water with a concentration of 100g/L. The dispersion underwent thorough stirring for 30 minutes at ambient temperature, after which the temperature was elevated to 80–90 °C until it reached a clear solution. Then $MoS_2$+PVA gel was prepared with a 1:1 ratio and stirring with 500 rpm for three hours under 80 °C. On one textile-based graphene printed electrode, 2ml of $MoS_2$+PVA gel composite was drop casted and dispersed over of the graphene, which was then dried for an hour in an ambient atmosphere before being covered with Kapton tape. Insulator-coating materials were printed over the other textile-based graphene electrode, acting as both an encapsulation and a triboelectric layer. Both sides of the T-TENGs were then joined using a sponge as a spacer and double-sided adhesive tape.

## T-Supercap Fabrication

Graphene electrode was printed on textile substrate in-plane symmetrical shape using manual screen printer and dried for 10 minutes under 80 °C. The PVA gel electrolyte was developed by dissolving polyvinyl alcohol (PVA) in an aqueous solution of $H_2SO_4$ (50 g/L). The solution was stirred constantly at room temperature for 60 minutes and then heated to 80 °C with continues stirrer 500 to 700 rpm till produce a clear solution. A 1.5 ml volume of PVA gel electrolyte was drop casted over the graphene electrode and dried before being wrapped with very flexible and transparent single-sided adhesive tape.

## Characterization Instrumentation

A force applicator was developed in the laboratory using CNC and 3D printing machines. It incorporates a mechanism to convert rotary motion into linear motion using a 24V DC motor, facilitating the exertion of force on the T-TENG. To measure the exerting force a commercial force measuring device was utilized in parallel **(Figure S4, supporting information)**. The output voltage was measured using a Tektronix TBS1052B oscilloscope, while current measurements were taken with a Keithley DMM 7510 multimeter. Rectifier and voltage-divider circuits were constructed in the lab for this purpose. For the electrochemical characterization of supercapacitors, an Iviumstat electrochemical interface was utilized. In the application for step counting, an Arduino UNO controller was programmed and interfaced with a desktop application developed in Python. Additionally, the surface morphology of fabricated layers was examined using an FEI Quanta 650 field emission scanning electron microscope (SEM).

## Supporting Information

Supporting information are available online.

## Acknowledgements

The authors kindly acknowledge funding from the UWE partnership PhD scheme, and UKRI Research England the Expanding Excellence in England (E3) grant. The authors also grateful for the support from Michael White and Nathan Townsend for their technical help in developing the force applicator and force measuring system, as well as David Patton for his assistance with SEM imaging.

## References


[1] A. Libanori, G. Chen, X. Zhao, Y. Zhou, J. Chen, *Nature Electronics* **2022**, 5, 142.

[2] H. C. Ates, P. Q. Nguyen, L. Gonzalez-Macia, E. Morales-Narváez, F. Güder, J. J. Collins, C. Dincer, *Nature Reviews Materials* **2022**, 7, 887.

[3] I. Ali, M. Dulal, N. Karim, S. Afroj, *Small Structures* **2024**, 5, 2300282.

[4] I. Ali, G. Hassan, A. Shuja, *Journal of Materials Science: Materials in Electronics* **2022**, 33, 3982.

[5] A. Chang, C. Uy, X. Xiao, X. Xiao, J. Chen, *Nano Energy* **2022**, 98, 107282.

[6] M. R. Islam, S. Afroj, J. Yin, K. S. Novoselov, J. Chen, N. Karim, *Advanced Science*, n/a, 2304140.

[7] S. Xiang, G. Chen, Q. Wen, H. Li, X. Luo, J. Zhong, S. Shen, A. Di Carlo, X. Fan, J. Chen, *Matter* **2024**, 7, 82.

[8] C. Xu, Y. Song, M. Han, H. Zhang, *Microsystems & Nanoengineering* **2021**, 7, 25.

[9] J. Zou, M. Zhang, J. Huang, J. Bian, Y. Jie, M. Willander, X. Cao, N. Wang, Z. L. Wang, *Advanced Energy Materials* **2018**, 8, 1702671.

[10] M. R. Islam, S. Afroj, N. Karim, *ACS Nano* **2023**, 17, 18481.

[11] D. Choi, Y. Lee, Z.-H. Lin, S. Cho, M. Kim, C. K. Ao, S. Soh, C. Sohn, C. K. Jeong, J. Lee, M. Lee, S. Lee, J. Ryu, P. Parashar, Y. Cho, J. Ahn, I.-D. Kim, F. Jiang, P. S. Lee, G. Khandelwal, S.-J. Kim, H. S. Kim, H.-C. Song, M. Kim, J. Nah, W. Kim, H. G. Menge, Y. T. Park, W. Xu, J. Hao, H. Park, J.-H. Lee, D.-M. Lee, S.-W. Kim, J. Y. Park, H. Zhang, Y. Zi, R. Guo, J. Cheng, Z. Yang, Y. Xie, S. Lee, J. Chung, I.-K. Oh, J.-S. Kim, T. Cheng, Q. Gao, G. Cheng, G. Gu, M. Shim, J. Jung, C. Yun, C. Zhang, G. Liu, Y. Chen, S. Kim, X. Chen, J. Hu, X. Pu, Z. H. Guo, X. Wang, J. Chen, X. Xiao, X. Xie, M. Jarin, H. Zhang, Y.-C. Lai, T.

He, H. Kim, I. Park, J. Ahn, N. D. Huynh, Y. Yang, Z. L. Wang, J. M. Baik, D. Choi, *ACS Nano* **2023**, 17, 11087.

[12] L. Long, W. Liu, Z. Wang, W. He, G. Li, Q. Tang, H. Guo, X. Pu, Y. Liu, C. Hu, *Nature Communications* **2021**, 12, 4689.

[13] I. Ali, M. R. Islam, J. Yin, S. J. Eichhorn, J. Chen, N. Karim, S. Afroj, *ACS Nano* **2024**.

[14] Z. Wen, M.-H. Yeh, H. Guo, J. Wang, Y. Zi, W. Xu, J. Deng, L. Zhu, X. Wang, C. Hu, L. Zhu, X. Sun, Z. L. Wang, *Science Advances* **2016**, 2, e1600097.

[15] J. Yin, S. Wang, A. Di Carlo, A. Chang, X. Wan, J. Xu, X. Xiao, J. Chen, *Med-X* **2023**, 1, 3.

[16] J. Yi, K. Dong, S. Shen, Y. Jiang, X. Peng, C. Ye, Z. L. Wang, *Nano-Micro Letters* **2021**, 13, 103.

[17] G. Chen, X. Xiao, X. Zhao, T. Tat, M. Bick, J. Chen, *Chemical Reviews* **2022**, 122, 3259.

[18] J. Luo, W. Gao, Z. L. Wang, *Advanced Materials* **2021**, 33, 2004178.

[19] F. Yi, H. Ren, J. Shan, X. Sun, D. Wei, Z. Liu, *Chemical Society Reviews* **2018**, 47, 3152.

[20] G. Pace, A. E. del Rio Castillo, A. Lamperti, S. Lauciello, F. Bonaccorso, *Advanced Materials* **2023**, 35, 2211037.

[21] Z. Lin, B. Zhang, Y. Xie, Z. Wu, J. Yang, Z. L. Wang, *Advanced Functional Materials* **2021**, 31, 2105237.

[22] Y. Teng, H. Zhao, Z. Zhang, Z. Li, Q. Xia, Y. Zhang, L. Zhao, X. Du, Z. Du, P. Lv, K. Świerczek, *ACS Nano* **2016**, 10, 8526.

[23] H. Hwang, K. Y. Lee, D. Shin, J. Shin, S. Kim, W. Choi, *Applied Surface Science* **2018**, 442, 693.

[24] C. Li, Y. Bai, J. Shao, H. Meng, Z. Li, *Small Methods*, n/a, 2301682.

[25] P. C. Uzabakiriho, Z. Haider, K. Emmanuel, R. u. S. Ahmad, A. Haleem, U. Farooq, J. D. D. Uwisengeyimana, M. K. Mbogba, A. Fareed, K. Memon, I. Khan, P. Hu, G. Zhao, *Advanced Materials Technologies* **2020**, 5, 2000303.

[26] C. Liu, Y. Bai, Y. Zhao, H. Yao, H. Pang, *Energy Storage Materials* **2020**, 33, 470.

[27] G. Pace, A. Ansaldo, M. Serri, S. Lauciello, F. Bonaccorso, *Nano Energy* **2020**, 76, 104989.

[28] S. Hasan, A. Z. Kouzani, S. Adams, J. Long, M. A. P. Mahmud, *Journal of Electrostatics* **2022**, 116, 103685.

[29] A. Y. Choi, C. J. Lee, J. Park, D. Kim, Y. T. Kim, *Scientific Reports* **2017**, 7, 45583.

[30] J. Xiong, P. Cui, X. Chen, J. Wang, K. Parida, M.-F. Lin, P. S. Lee, *Nature Communications* **2018**, 9, 4280.

[31] W. Paosangthong, M. Wagih, R. Torah, S. Beeby, *Nano Energy* **2019**, 66, 104148.

[32] J. Liu, L. Gu, N. Cui, Q. Xu, Y. Qin, R. Yang, *Research* **2019**, 2019.

[33] W. Sangkhun, S. Wanwong, *Nanoscale* **2021**, 13, 2420.

[34] W. Paosangthong, M. Wagih, R. Torah, S. Beeby, *Nano Energy* **2022**, 92, 106739.

[35] I. Domingos, Z. Saadi, K. S. Sadanandan, H. A. Pocinho, D. M. Caetano, A. I. S. Neves, M. F. Craciun, H. Alves, *Nano Energy* **2023**, 115, 108688.

[36] D. E. Kim, S. Shin, G. Zhang, D. Choi, J. Jung, *RSC Advances* **2023**, 13, 11142.

[37] J. Huang, S. Wang, X. Zhao, W. Zhang, Z. Chen, R. Liu, P. Li, H. Li, C. Gui, *Materials Horizons* **2023**, 10, 3840.

[38] M. R. Islam, S. Afroj, C. Beach, M. H. Islam, C. Parraman, A. Abdelkader, A. J. Casson, K. S. Novoselov, N. Karim, *IScience* **2022**, 25.